AIMS Materials Science, 11(3): 547–564.
DOI: 10.3934/matersci.2024027
Received: 28 March 2024
Revised: 14 May 2024
Accepted: 15 May 2024
Published: 22 May 2024

https://www.aimspress.com/journal/Materials

Research article

The effect of the electrolyte composition on the microstructure and properties of coatings formed on a titanium substrate by microarc oxidation

Bauyrzhan Rakhadilov[1,2], Ainur Zhassulan[1,*], Daryn Baizhan[1], Aibek Shynarbek[1], Kuanysh Ormanbekov[1] and Tamara Aldabergenova[1]

[1] Shakarim University NJSC, "Surface Modification of Materials" SC, Semey 071412, Kazakhstan
[2] PlasmaScience LLP, Ust-Kamenogorsk 070000, Kazakhstan

*** Correspondence:** Email: info@semgu.kz; Tel: +7-778-984-9467.

Abstract: This article is dedicated to investigating the impact of different electrolyte compositions on the development of titanium coatings endowed with superior mechanical, tribological, and corrosion properties. An experimental analysis was conducted on three distinct electrolyte formulations, each contributing unique attributes to the coating's structural formation. Advanced analytical techniques, including scanning electron microscopy, hardness testing, wear resistance evaluation, and corrosion trials in harsh environments, were employed to gauge the mechanical, tribological, and anti-corrosive performance of the coatings. The utilization of scanning electron microscopy, X-ray structural analysis, and additional methodologies enabled an in-depth characterization of the microstructure and elucidated the relationship between the physico-mechanical properties and the electrolyte's chemical makeup. Among the electrolytes examined, the composition containing potassium hydroxide emerged as superior, fostering coatings with a distinctively porous structure that augment mechanical attributes. A considerable degree of porosity coupled with relatively small pore dimensions suggests the potential to engineer structures that exhibit optimal mechanical robustness. Furthermore, research findings related to this specific electrolyte composition revealed enhancements in the friction coefficient and wear resistance, indicating its promising prospects for tribological applications. The study also meticulously addressed the corrosion aspects, revealing that the microarc oxidation-derived coatings substantially improve corrosion resistance by offering more favorable potentials and currents than the bare titanium substrate. The efficacy of microarc oxidation as an avant-garde technique to advance the

properties of titanium alloys underscores its prospective utility and practical relevance in contemporary industrial applications.

Keywords: coating; titanium; microarc oxidation; electrolyte; microhardness; wear resistance; corrosion

1. Introduction

Titanium and its alloys are utilized in aerospace, marine, and biomedical fields due to their low density, good electrical and thermal conductivity, and ease of mechanical processing [1,2]. While they generally offer satisfactory wear resistance, they can undergo accelerated wear under extreme operating conditions [3–6]. Wear resistance is particularly crucial for titanium-based medical implants and prostheses, which must endure persistent mechanical stresses. Moreover, although biocompatible, these materials sometimes show suboptimal osseointegration, necessitating surface modifications to enhance bone tissue interaction [2,7]. Surface treatments such as plasma chemical deposition, thermal oxidation, anodizing, and chemical vapor deposition create thin films on titanium surfaces. However, these methods fall short in producing coatings with the desired porosity and thickness control that are essential for improved corrosion resistance and durability against intense wear [8–11].

Microarc oxidation (MAO), also referred to as plasma electrolytic oxidation (PEO), is an efficacious surface treatment technique that enhances the hardness and wear resistance of titanium and its alloys through the formation of ceramic coatings [12,13]. MAO significantly improves the wear resistance of coatings, rendering titanium alloys more suitable for biomedical applications such as implants and prostheses. This enhancement is achieved by forming oxide coatings on the titanium surface, which not only improve the tribological properties but also offer augmented protection against corrosion. MAO generates a thin yet robust oxide layer and can yield structurally complex coatings, which play a critical role in enhancing biocompatibility and promoting osseointegration [14–19].

To further enhance the properties of titanium alloys, selecting the appropriate electrolytes is crucial. A variety of acidic, saline, and alkaline electrolytes can be employed for MAO treatments on titanium and titanium alloys, such as silicates, potassium fluoride, sodium hydroxide, sodium tetraborate, and sodium phosphate, among others. For instance, sodium hydrogen phosphate (Na_2HPO_4), as utilized in reference [20], was shown to produce coatings that not only reduce corrosion rates but also exhibit biological activity. Moreover, the inclusion of phosphoric acid and powders of hydroxyapatite and wollastonite in the electrolyte solution has been found to increase the osteogenic potential of fibroblast-like cells adhering to a Ti40Nb alloy, attributable to alkaline phosphatase activity [21]. An electrolyte solution containing calcium carbonate ($CaCO_3$) has been demonstrated to yield coatings on magnesium substrates with favorable anticorrosive and self-healing properties [22]. Research in [23] revealed that adding sodium orthophosphate (Na_3PO_4) to the baseline electrolyte was sufficient to augment the chemical and mechanical resistance of the MAO coatings without affecting their surface roughness and thickness. The most commonly employed electrolyte for MAO is a mixed phosphate-alkaline solution, specifically KOH-Na_3PO_4. Studies [24,25] have explored how the electrolyte composition influences the intensity and size of microdischarges, as well as the volume of gas evolution. In the KOH-Na_3PO_4 mixture, potassium hydroxide (KOH) serves as an activator that facilitates enrichment, leading to the formation of a reinforcing layer on the oxidized surface. The enhanced corrosion resistance of samples processed with equal proportions of silicate and KOH is

likely due to increased coating thickness, less porous surface morphology, and higher resistance of the internal barrier layer [26]. Coatings containing aluminates display a volcanic morphology characterized by a mix of nodular particles and craters across the surface. Phosphate-based coatings exhibit a sintered structure replete with craters, alongside an uneven distribution of micropores and microcracks, which are linked to porosity. Silicate-containing coatings are distinguished by their highly porous framework, constituted by a network of micropores and oxide granules [27]. Phosphate-based electrolytes are considered the most promising, given their superior efficiency in forming coatings and the lowest breakdown voltage [28]. While most substances within the coating are not directly involved in plasma reactions, chemical, electrochemical, and thermally induced reactions are predominant in coating formation [29]. The type of electrolyte significantly influences the Ca/P ratio in MAO coatings because different electrolytes affect the incorporation and distribution of calcium and phosphorus within the coatings. Study [30] examines a PEO process in which various metal oxides are incorporated into the coating, affecting not only corrosion resistance but also, potentially, the chemistry, including the Ca/P ratio. Double introduction of molybdenum oxide (MoO_2) and silicon oxide (SiO_2) affects the protective properties of coatings, which can indirectly affect the Ca/P ratio due to changes in the electrolyte composition and interaction dynamics during the PEO process [31]. Although this study primarily focuses on mechanical properties, it shows how changes in electrolyte components (e.g., titanium oxide (TiO_2) nanoparticles) can alter surface characteristics and underlying chemical structures, possibly affecting the Ca/P ratio [32]. Combining the data from these studies, it becomes clear that the type of electrolyte and the additives used (such as TiO_2, MoO_2, and SiO_2 nanoparticles) significantly influence the elemental composition and distribution within PEO coatings. This effect extends to the Ca/P ratio, which can vary depending on how these elements are incorporated into coatings during the PEO process. Changes in the Ca/P ratio are critical as they can affect the mechanical properties and biocompatibility of coatings, which are especially important in biomedical applications [30–33].

Previous research has demonstrated that MAO treatment enhances the performance of various alloy coatings. This suggests that the electrolyte composition is a critical factor in improving the properties of these coatings. Despite these advances, there remains a notable lack of detailed studies on the mechanical and tribological properties of MAO coatings applied to VT1-0 titanium substrates. Furthermore, comprehensive investigations into how the electrolyte composition correlates with coating properties—knowledge crucial for practical applications—are sparse [34–36]. In the present study, phosphates and calcium carbonates were employed as the primary components in the MAO electrolytes for modifying VT1-0 alloys. This research is focused on assessing the impact of the resulting coatings on the microstructure and corrosion resistance when applied to VT1-0 alloys via MAO. Given the direct influence of coating properties on the performance of the materials in service, the insights gained from this study are of substantial practical significance [37–40]. The aim of this article is to explore the influence of different electrolyte compositions on the mechanical, tribological, and corrosion properties of titanium coatings fabricated through the MAO technique.

2. Materials and methods

The coating using the MAO method was applied with a pulsed power supply, specifically a KP-HI-F-40A 600V rectifier. The MAO apparatus comprises a programmable switching power supply, an electrochemical bath with cooling capabilities, and a set of electrodes (Figure 1). Overall, the

operational setup for the MAO process includes: power equipment—namely, the power supply; baths for surface preparation, treatment, and rinsing; and auxiliary equipment such as cooling systems.

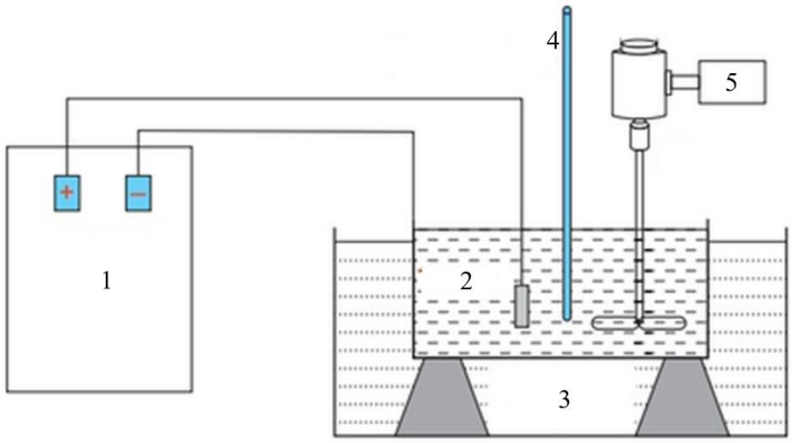

Figure 1. Schematic diagram of the microarc oxidation setup: 1-power supply, 2-sample, 3-condensed water, 4-thermometer, 5-stirrer.

The parameters of the MAO process for this work are presented in Table 1. According to the literature, 300 V was chosen as the optimal voltage parameter for MAO [41,42]. When performing MAO, the current is in the range of 0.50–0.70 A. Samples of titanium alloy VT1-0 with dimensions 2 × 2 × 2 cm, pre-polished and prepared for the experiment, were used as the substrate material. The current density was calculated using the Eq 1:

$$J = \frac{I}{A} \tag{1}$$

where I is the current in amperes, and A is the surface area in square meters through which the current passes.

Table 1. Technological parameters of the MAO.

Frequency, Hz	Voltage, V	Current density, A/cm^2	Time, sec	Pulse duration, mks
100	300	0.13–0.17	600	100

In accordance with the object of study, three different electrolyte compositions were selected, as shown in Table 2. The samples were immersed in an aqueous solution (500 mL of distilled water) of the electrolyte and microarc oxidation was carried out.

Table 2. Electrolyte composition for the MAO process.

Regimes	Electrolyte
No. 1	Na_2HPO_4 (5 g), hydroxyapatite (HA) (2 g), KOH (2 g)
No. 2	H_3PO_4 (15%), HA (2 g), $CaCO_3$ (5 g)
No. 3	Na_3PO_4 (5 g), HA (3 g), $CaCO_3$ (5 g)

The surface morphology of the coatings was examined using a fourth generation TESCAN VEGA scanning electron microscope with a thermionic tungsten cathode. To calculate porosity, the ImageJ software package, designed for image processing and analysis, was used. The phase composition of the coatings was studied by X-ray diffraction (XRD) analysis using an X-pertPRO X-ray diffractometer using CuKα radiation (1.5406 Å) in standard Bragg–Brentano geometry. The following parameters were used for X-ray diffraction measurements: X-ray tube voltage—40 kV, X-ray tube current—30 mA, scan angle range—20–60°, scan step size—0.0200, and signal acquisition time—1 s. The roughness of the coatings was measured using a HY2300 Anytester profilometer. The sample is installed on the profilometer table. It is important to properly align the sample so that the surface is parallel to the direction of the probe movement. The profilometer probe, which is usually a microscopically thin needle, contacts the surface of the sample and moves along a specified area. In this case, the probe records the vertical movement necessary to maintain contact with the surface, which allows the generation of a roughness profile. Hardness determination was carried out using the FISCHERSCOPE HM2000 S measuring system in accordance with the requirements of the DIN EN ISO 14577-1 standard. A load of 300 mN was chosen for testing. Primary processing of the test results was carried out using the software of the WIN-HCU device. A tetrahedral Vickers diamond pyramid with a plane angle of 136° was used as an indenter. Tribological tests were carried out under the following conditions: load up to 3 N, speed—2.5 cm/s, radius—2 mm, ball radius (silicon nitride (Si_3N_4) counterbody) —3 mm. Corrosion tests were carried out by the potentiodynamic method using a single-channel potentiostat-galvanostat model CS300M in a 3.5% sodium chloride (NaCl) solution at a temperature of ±25 ℃. To obtain the area under study, materials such as tape and varnish were used; a protective coating of varnish was used to isolate the area of the sample not being studied. To enable comparison of the results when conducting potentiodynamic studies, it is extremely important that the analyzed areas on the tested samples are identical. This is necessary so that the values obtained during testing of the samples under the same conditions are comparable. In one glass cell, there is a reference electrode (R) with a known constant potential—a silver chloride electrode filled with a NaCl solution with a pH value of 6, and in the second cell, there is an auxiliary electrode (C)—a platinum electrode and a working electrode (W)—the test titanium samples with and without coatings with a surface area of 0.25 cm^2. The cells are connected by a salt bridge containing sodium chloride and both sides are covered with filter paper, designed to prevent the mixing of solutions in the cells. This is necessary to ensure accurate potential measurements as mixing may affect the results. Before installing the test sample into the circuit, it is prepared by cleaning and removing greasy contaminants using ethyl alcohol. The CS Studio6 program allows you to determine the values of the potential, current density, corrosion rate, as well as Tafel slopes (ba, bc). The graphs are presented in logarithmic form (the current density scale is presented in logarithmic form). In addition, it provides the ability to visually monitor the construction of curves of value changes on a computer.

3. Results and discussion

3.1. Investigation of porosity and morphology of the surface of MAO coatings

The surface morphology of the coatings is shown in Figure 2. During the investigation of the surface morphology of the coatings, a noticeable difference in structure and porosity was observed between the used electrolyte compositions. For further examination of the surface and to achieve

additional functional properties of titanium, MAO was performed in various electrolytes. As a result of these processes, as presented in Figure 2 (a, b, and c), noticeable changes in surface morphology and the formation of oxide layers with unique properties were observed.

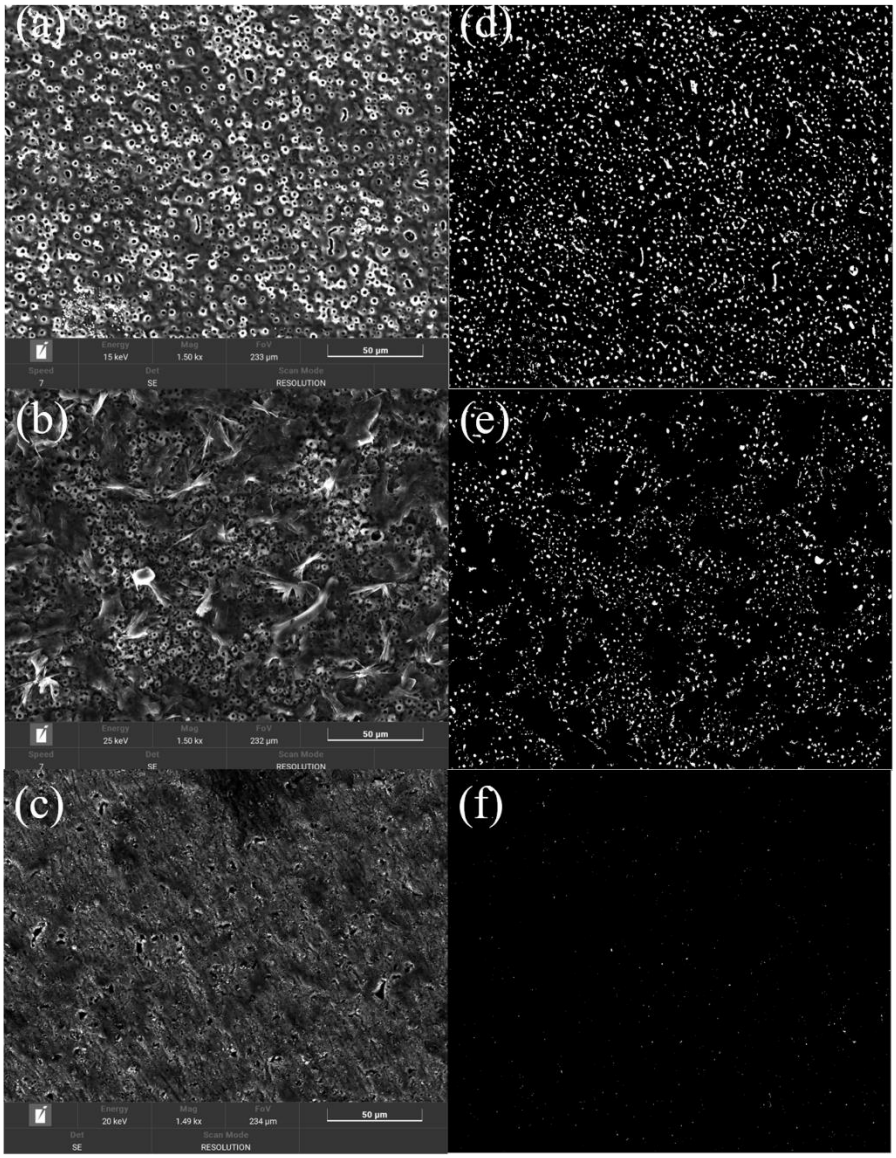

Figure 2. The microstructure of the surface of MAO coatings in various electrolytes with an increase of ×1500: (a) electrolyte No. 1, (b) electrolyte No. 2, (c) electrolyte No. 3, and micropore images obtained using the ImageJ software package: (d) electrolyte No. 1, (e) electrolyte No. 2, (f) electrolyte No. 3.

The resulting coating using electrolyte No. 1 showed a more pronounced porous structure. This porosity may be due to a combination of electrolyte components, including KOH, which contributes to the formation of pores in the oxide layer. The process involving KOH can lead to the formation of a porous structure in oxide coatings [43,44]. Gases released as a result of reactions on the surface create micropores in the resulting oxide films. This effect was further enhanced by the choice of certain electrolyte formulations, such as Na_2HPO_4 [45], which contain components that promote the formation

of gases. The coating obtained using electrolyte No. 2 has a less pronounced porous structure. The presence of H_3PO_4 in the electrolyte contributes to the formation of a denser and more compact oxide layer [46]. It is also worth noting that with this electrolyte composition, the oxidation process was actively proceeding, resulting in pronounced macro-irregularities with holes. Unlike coatings with electrolytes No. 1 and No. 2, the coating using electrolyte No. 3 does not exhibit noticeable porosity. This can be explained by the balance between Na_3PO_4, HA, and $CaCO_3$, which ensures the formation of a denser oxide layer. The absence of pores indicates a more structurally compact nature for this coating. Large sparks lead to the formation of large and small micropores, while smaller sparks form smaller micropores and, as a result, form a more homogeneous structure [47].

The average size of micropores and the percentage of porosity are shown in Table 3. Porosity was measured using ImageJ, a versatile and powerful image analysis software widely used in the scientific community and particularly useful for analyzing the porosity of materials using microscopic images. This process provides a quantitative measurement of porosity, which is important in materials science for applications such as assessing the structural integrity and characteristics of materials, and for other purposes [48–50]. According to Figure 2, the pores are evenly distributed and have the same size. Electrolyte No. 2 (Figure 2e) is characterized by visible large pores shaped as large spheres, which were formed as a result of an active oxidation process due to the concentration of orthophosphoric acid in the electrolyte.

Table 3. Porosity values of the obtained coatings.

Electrolyte	Average pore size, μm	Percentage of porosity, %
No. 1: Na_2HPO_4 (5 g), HA (2 g), KOH (2 g)	2.21	9.5
No. 2: H_3PO_4 (15%), HA (2 g), $CaCO_3$ (5 g)	4.78	4.9
No. 3: Na_3PO_4 (5 g), HA (3 g), $CaCO_3$ (5 g)	0.003	0.2

3.2. Elemental and X-ray diffraction analysis

An important point is the elemental analysis (Figure 3), which revealed the presence of elements such as calcium, phosphorus, oxygen, and sodium, which make up the electrolyte and the substrate material, titanium. The absence of pronounced phases of these elements can be explained by their low mass content, as well as the amorphousness of the thin coatings obtained during MAO [51–55].

The mechanism of formation of MAO coatings on Ti substrates was revealed using energy dispersive X-ray spectroscopy (EDS) analysis. The MAO coating contained Ti, O, Ca, P, and Na. Na was obtained from the electrolyte. The Ti content was 56.92 wt.%, showing that the electrolyte affects the color and properties of the coating. In our study, two forms of sodium phosphate were used across different electrolytes: Na_2HPO_4, a dibasic sodium phosphate in No. 1, and Na_3PO_4, a tribasic sodium phosphate in No. 3. Tribasic sodium phosphate generally exhibits higher solubility and a greater rate of dissociation in aqueous solutions compared to its dibasic counterpart [56]. This leads to a significantly enhanced availability of sodium ions during electrolysis with No. 3, thereby increasing their likelihood of being incorporated into the coating. Conversely, the presence of KOH in No. 1 increases the pH, which may induce precipitation of some sodium ions as less soluble compounds, reducing the availability of free sodium ions for incorporation into the coating. In No. 3, $CaCO_3$ reacts

with phosphate ions to form calcium phosphate, thereby maintaining a higher concentration of free sodium ions in the solution, which facilitates their deposition onto the substrate.

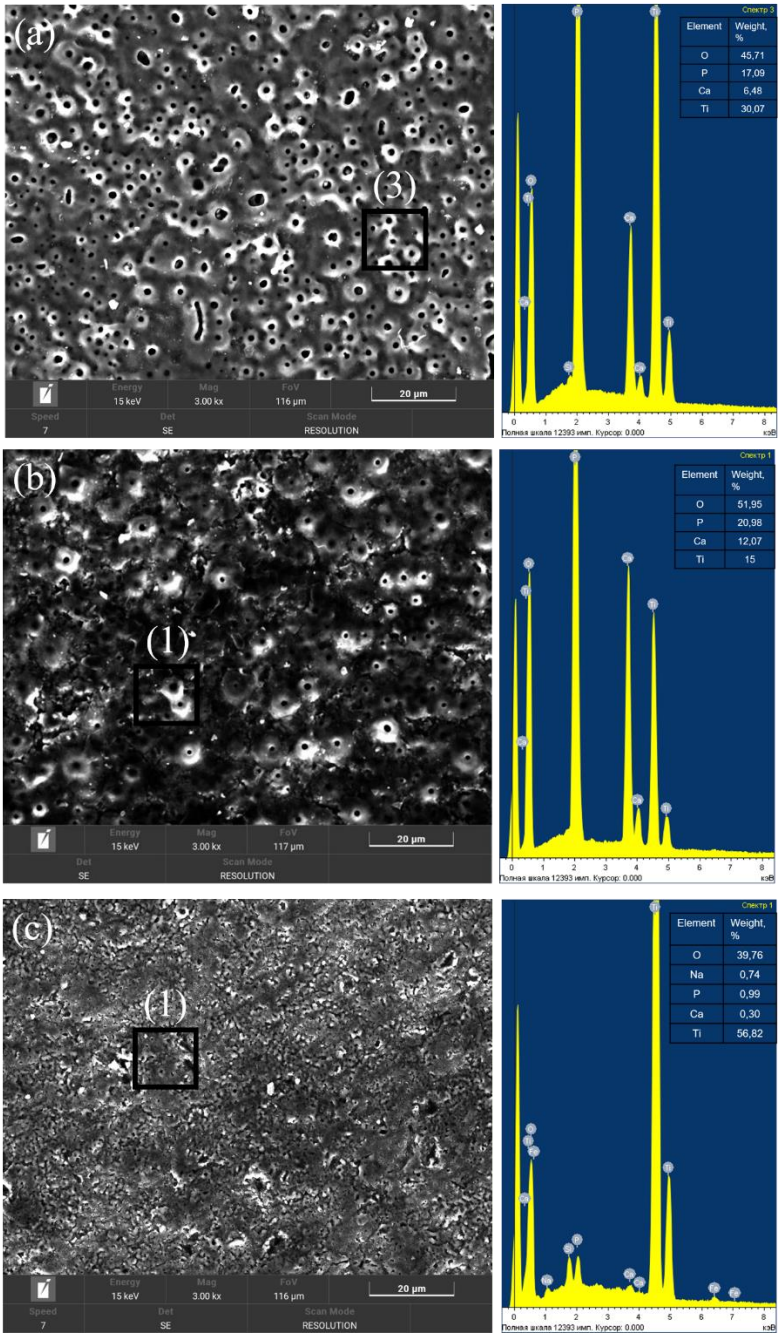

Figure 3. EDS spectra with indication of the place where the spectrum was taken on MAO coatings: (a) electrolyte No. 1, (b) electrolyte No. 2, (c) electrolyte No. 3.

The X-ray image obtained from the surface of the coatings and the initial titanium is shown in Figure 4.

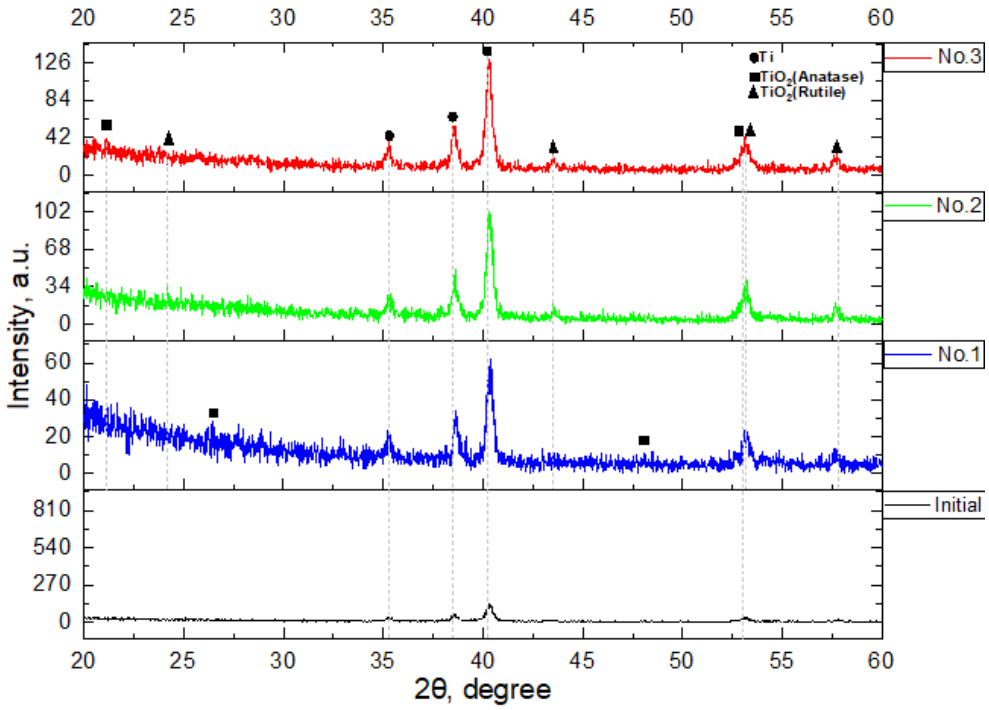

Figure 4. Diffractogram of samples before and after applying MAO coatings in various electrolytes.

Analysis of the diffraction patterns of coatings formed by electrolytes No. 1, No. 2, and No. 3 confirms the presence of rutile and anatase phases of titanium dioxide (TiO_2). These phases are formed as a result of the interaction of the titanium substrate with oxygen coming from electrolyte solutions during the MAO process. The detection of titanium crystal phases also highlights the efficiency of the processing and the formation of stable oxide layers.

3.3. Investigation of the mechanical and tribological properties of MAO coatings

The roughness value is shown in Table 4. The presence of irregularities is due to sandblasting before sample preparation. Consequently, no significant changes in surface roughness were detected. Electrolyte No. 2 has a higher roughness due to the formation of micro-irregularities on the surface.

Table 4. The roughness of the MAO coatings.

Regimes	Roughness (Ra), μm
Initial	3.13 ± 0.5
No. 1: Na_2HPO_4 (5 g), HA (2 g), KOH (2 g)	3.24 ± 0.9
No. 2: H_3PO_4 (15%), HA (2 g), $CaCO_3$ (5 g)	3.96 ± 0.8
No. 3: Na_3PO_4 (5 g), HA (3 g), $CaCO_3$ (5 g)	3.03 ± 0.2

Differences in the compositions of electrolytes lead to the formation of oxide coatings with different structures and properties. High values of microhardness indicate the effectiveness of the

MAO method in improving the mechanical properties of the surface of the material. The microhardness results are presented in Table 5.

Table 5. Microhardness of MAO coatings.

Regimes	$HV_{0.1}$	H, MPa	E, MPa
Initial	151.3 ± 1.0	15.4 ± 1.5	120.5 ± 1.5
No. 1: Na_2HPO_4 (5 g), HA (2 g), KOH (2 g)	327.8 ± 2.8	33.4 ± 1.2	153 ± 2.2
No. 2: H_3PO_4 (15%), HA (2 g), $CaCO_3$ (5 g)	267.1 ± 3.4	27.2 ± 2.1	115.2 ± 2.8
No. 3: Na_3PO_4 (5 g), HA (3 g), $CaCO_3$ (5 g)	291 ± 1.3	26.7 ± 1.1	132 ± 1.9

A significant increase in the microhardness of MAO coatings compared to the initial titanium indicates the formation of a solid oxide layer due to the formation of rutile and anatase phases. Rutile has a high hardness, and its preparation in coatings improves their mechanical properties, such as hardness and scratch resistance. The microhardness of electrolyte No. 1 is two times greater than the initial sample.

The coefficient of friction of the coatings obtained in the MAO process can vary depending on several factors, including the composition of the coating, surface roughness, environmental conditions, and the analog material with which the coating interacts. The coefficient of friction is an indicator of the slip resistance between two contacting surfaces and depends on both the internal properties of the coating and external factors [57,58]. Rutile, as a rule, has a higher hardness compared to anatase, which reduces wear and, thereby, the coefficient of friction in tribological systems. The measurement of the coefficient of friction for the first electrolyte was 0.109 μ, for the second was 0.133 μ, and for the third was 0.532 μ, compared to the initial uncoated titanium, which was 0.773 μ. The images show signs of wear resulting from the tribological testing of the surfaces of the original and coated samples. The initial sample (Figure 5a) shows significant wear, characterized by a long, deep scratch. This indicates significant material removal and path deformation, indicating aggressive wear conditions. The smoother surface with little wear on No. 1 (Figure 5b) indicates less wear and a more durable finish than the original. No. 2 (Figure 5c) shows signs of wear in the form of a blurred, spotted pattern. This suggests more distributed wear due to abrasive particles. No. 3 (Figure 5d) shows a wear pattern with a jagged edge. This morphology may indicate delamination or cracking of the material. It is worth noting that the surface of the third coating has fewer pores, which may not retain lubricant as effectively. These wear marks help evaluate the durability and resistance of surface treatments or coatings under simulated or actual operating conditions.

Figure 5 shows micrographs and surface profiles of the wear marks of the substrate before and after the MAO. It can be seen that the wear trace of the substrate of the initial titanium is wide and deep, which indicates a high degree of wear during tribological application. However, the wear mark of the MAO coating No. 1 becomes shallow and narrow. This clearly demonstrates the MAO coating's improvement in the titanium alloy's anti-wear properties and its very low coefficient of friction during slip tests. The increase in wear resistance is due to the compact microstructure and high hardness of the oxide ceramic coating.

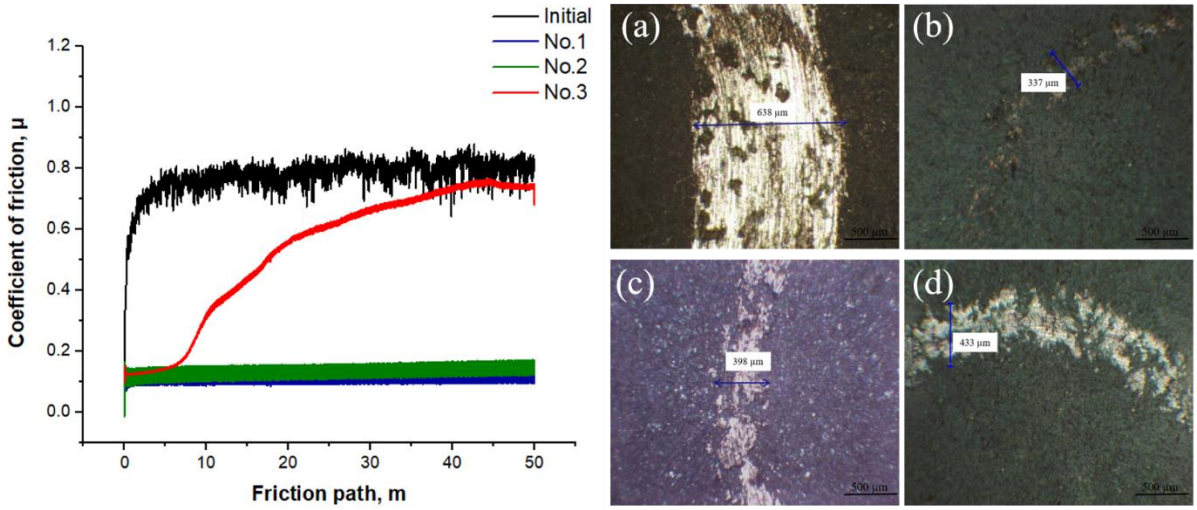

Figure 5. Tribological test results: (a) initial, (b) No. 1, (c) No. 2, (d) No. 3.

3.4. Investigation of the corrosion properties of MAO coatings

According to the results of the corrosion test, the values were obtained (Table 6), which show increases in the corrosion resistance of the samples after the MAO. During corrosion resistance studies, polarization curves were obtained (Figure 6). Titanium and its alloys have a strong tendency to form a protective oxide layer when exposed to an electrolyte, which can alter the electrochemical behavior, especially under anodic conditions. The change in linearity of the curves may reflect differences in the stability between samples. This passive film may be very thin, but is highly protective, causing the observed current density to decrease as the potential moves away from the corrosion potential. Moreover, the observed nonlinearity may also be influenced by the microstructure of the titanium alloy itself, including variations in alloying elements, grain size, and the presence of intermetallic phases, which can influence how uniformly the passive layer forms and behaves under anodic polarization [59].

Table 6. Electrochemical data of samples before and after MAO.

Samples	$-E_{corr}$, mB	I_{corr}, A/cm²	r_{corr}, mm/a	Tafel slopes, mV	
				ba	bc
Initial	218.87	6.0461E−06	0.12294	834.37	−361.68
No. 1	132.17	3.5191E−07	0.0041284	379.43	−86.935
No. 2	52.177	4.2888E−07	0.0050313	220.49	−359.68
No. 3	44.49	8.663E−07	0.010163	966.84	−170.35

The initial sample has the highest corrosion potential (least negative), indicating a relatively more noble behavior, but with a significant current density once it begins to corrode, suggesting that it may not be very resistant to corrosion in this environment. The curve of the initial titanium is the most negative, indicating that untreated titanium has the greatest tendency to corrosion under these test conditions. The anode slope is quite steep—834.37 mV, which indicates a strong dependence of the anode reaction on the potential. Electrolyte No. 1 is the most positive and flat of the curves, which

indicates better corrosion resistance, thanks to effective MAO treatment that has changed the properties of the surface. The anode and cathode slopes are lower, indicating more stable reactions on the electrode surface. Electrolyte No. 2 has a moderate improvement in corrosion resistance compared to the initial sample, but less effective than sample No. 1. Electrolyte No. 3 has improved corrosion resistance compared to the initial titanium, but worse than samples No. 1 and No. 2, which may indicate less effective microarc oxidation treatment in terms of corrosion resistance fortitude. The interaction of Na_2HPO_4 and KOH leads to the formation of more stable phosphate compounds on the titanium surface, which improves the quality of the MAO coating. High concentrations of H_3PO_4 can lead to a more aggressive MAO process, resulting in a less uniform coating. However, the presence of HA and $CaCO_3$ stabilizes the coating to some extent due to the formation of phosphate, which is known to have good bioactivity and corrosion resistance.

Overall, the treatment improved the corrosion resistance of the titanium samples, with sample No. 1 showing the most significant improvement. The exact nature of electrolyte compositions and their effect on surface characteristics will be important for understanding the causes of differences in electrochemical behavior. The corrosion resistance of titanium alloys is significantly influenced by the composition of the electrolyte used in the MAO process. Although all of the treated samples showed improvements over untreated titanium, differences in electrolyte components, such as phosphate sources, alkaline additives, and the presence of calcium compounds, play a critical role in determining the effectiveness of the corrosion resistance provided by MAO coatings. This expanded section provides greater insight into the corrosion behavior of titanium samples processed under various conditions, clearly relating electrolyte composition to observed electrochemical characteristics and offering a detailed explanation of the underlying mechanisms influencing the corrosion resistance of each sample. Installation using a reference electrode in one cell, a counter (platinum) and a working electrode (samples) in another, with a salt bridge connecting them, is standard for such measurements and allows for clear comparison of the samples.

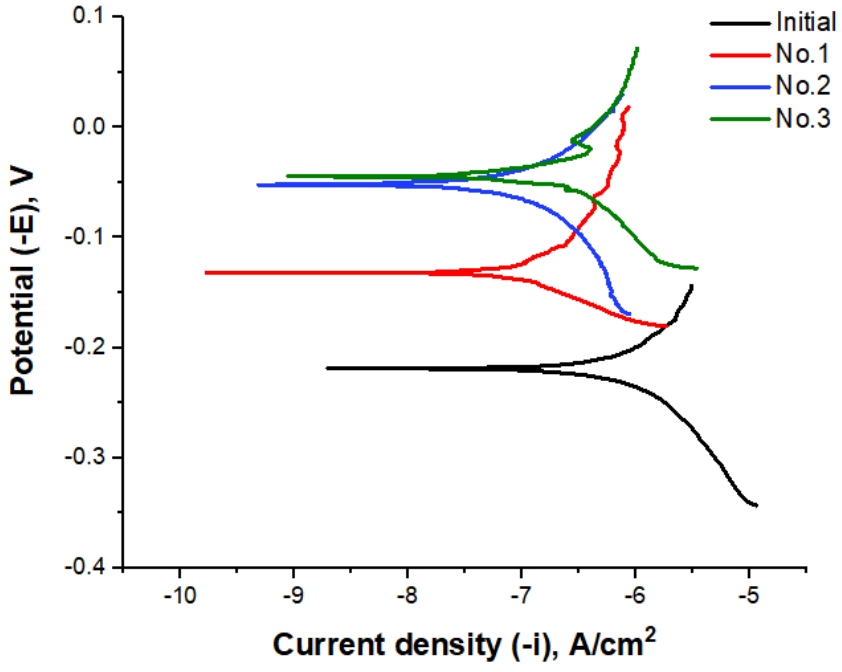

Figure 6. Diagram of electrochemical corrosion measurement results on the samples.

4. Conclusions

The study demonstrated the significant influence of the electrolyte composition on the quality and characteristics of coatings formed on titanium substrates using microarc oxidation. It was found that the variety of electrolytic compositions directly affects the microstructure, porosity, and mechanical properties of coatings, including microhardness and corrosion resistance. Particularly noteworthy was the role of the electrolyte with the addition of KOH, which contributed to the formation of highly porous coatings with improved mechanical properties. These coatings demonstrated not only improved mechanical properties, but also increased wear resistance and corrosion resistance compared to the original titanium.

This study confirms that microarc oxidation is an effective technology for improving the performance of titanium alloys, making it promising for use in industrial and biomedical applications. The results of this work expand the understanding of the relationship between electrolyte chemistry and coating properties, which may facilitate the development of new electrolyte compositions for targeted control of coating properties.

This study also highlights the need for further detailed studies of the mechanical and tribological properties of coatings created by microarc oxidation to ensure their practical application in various operating conditions.

Use of AI tools declaration

The authors declare that they have not used artificial intelligence (AI) tools in the creation of this article.

Author contributions

Main experimental work and data analysis: A.Zh. and D.B.; methodology: A.Sh. and K.O; project administration: B.R. and T.A.; writing—original draft: B.R. and A.Zh.; writing—review and editing: A.Zh. All authors have read and agreed to the published version of the manuscript.

Acknowledgments

This research has been funded by the Science Committee of the Ministry of Science and Higher Education of the Republic of Kazakhstan (Grant No. AP13068451).

Conflict of interest

The authors declare no conflict of interest.

References

1. Geetha M, Singh AK, Asokamani R, et al. (2009) Ti based biomaterials, the ultimate choice for orthopaedic implants—A review. *Prog Mater Sci* 54: 397–425. https://doi.org/10.1016/j.pmatsci.2008.06.004

2. Chen QZ, Thouas GA (2015) Metallic implant biomaterials. *Mater Sci Eng R* 87: 1–57. https://doi.org/10.1016/j.mser.2014.10.001
3. Vieira AC, Ribeiro AR, Rocha LA, et al. (2006) Influence of pH and corrosion inhibitors on the tribocorrosion of titanium in artificial saliva. *Wear* 261: 994–1001. https://doi.org/10.1016/j.wear.2006.03.031
4. Souza JCM, Henriques M, Teughels W, et al. (2015) Wear and corrosion interactions on titanium in oral environment: Literature review. *J Bio Tribo Corros* 1: 13. https://doi.org/10.1007/s40735-015-0013-0
5. Shokouhfar M, Allahkaram SR (2017) Effect of incorporation of nanoparticles with different composition on wear and corrosion behavior of ceramic coatings developed on pure titanium by micro arc oxidation. *Surf Coat Technol* 309: 767–778. https://doi.org/10.1016/j.surfcoat.2016.10.089
6. Ao N, Liu DX, Wang SX, et al. (2016) Microstructure and tribological behavior of a TiO_2/hBN composite ceramic coating formed via microarc oxidation of Ti–6Al–4V alloy. *J Mater Sci Technol* 32: 1071–1076. https://doi.org/10.1016/j.jmst.2016.06.015
7. Zhang B, Pei X, Zhou C, et al. (2018) The biomimetic design and 3D printing of customized mechanical properties porous Ti6Al4V scaffold for load-bearing bone reconstruction. *Mater Design* 152: 30–39. https://doi.org/10.1016/j.matdes.2018.04.065
8. Kang S, Mauchauffé R, You YS, et al. (2018) Insights into the role of plasma in atmospheric pressure chemical vapor deposition of titanium dioxide thin films. *Sci Rep* 8: 16684. https://doi.org/10.1038/s41598-018-35154-4
9. Redmore E, Li X, Dong H (2019) Tribological performance of surface engineered low-cost beta titanium alloy. *Wear* 426: 952–960. https://doi.org/10.1016/j.wear.2019.01.032
10. İzmir M, Ercan B (2019) Anodization of titanium alloys for orthopedic applications. *Front Chem Sci Eng* 13: 28–45. https://doi.org/10.1007/s11705-018-1759-y
11. Khanna S, Patel R, Marathey P, et al. (2020) Growth of titanium dioxide nanorod over shape memory material using chemical vapor deposition for energy conversion application. *Mater Today Proc* 28: 475–479. https://doi.org/10.1016/j.matpr.2019.10.035
12. Jin J, Li XH, Wu JW, et al. (2018) Improving tribological and corrosion resistance of Ti6Al4V alloy by hybrid microarc oxidation/enameling treatments. *Rare Met* 37: 26–34. https://doi.org/10.1007/s12598-015-0644-9
13. Wei K, Chen L, Qu Y, et al. (2019) Tribological properties of microarc oxidation coatings on Zirlo alloy. *Surf Eng* 35: 692–700. https://doi.org/10.1080/02670844.2019.1575001
14. Liu L, Zeng D, Chen Y, et al. (2020) Microarc oxidation surface of titanium implants promote osteogenic differentiation by activating ERK1/2-miR-1827-Osterix. *In Vitro Cell Dev Biol-Animal* 56: 296–306. https://doi.org/10.1007/s11626-020-00444-7
15. Wu Y, Zhu B, Zhang X, et al. (2022) Preparation and characterization of Y-doped microarc oxidation coating on AZ31 magnesium alloys. *J Biomater Appl* 37: 930–941. https://doi.org/10.1177/08853282221121886
16. Butt MS, Maqbool A, Saleem M, et al. (2020) Revealing the effects of microarc oxidation on the mechanical and degradation properties of Mg-based biodegradable composites. *ACS Omega* 5: 13694–13702. https://doi.org/10.1021/acsomega.0c00836

17. Chen J, Li J, Hu F, et al. (2019) Effect of microarc oxidation-treated Ti6Al4V scaffold following low-intensity pulsed ultrasound stimulation on osteogenic cells in vitro. *ACS Biomater Sci Eng* 5: 572–581. https://doi.org/10.1021/acsbiomaterials.8b01000
18. Yuan W, Li B, Chen D, et al. (2019) Formation mechanism, corrosion behavior, and cytocompatibility of microarc oxidation coating on absorbable high-purity zinc. *ACS Biomater Sci Eng* 5: 487–497. https://doi.org/10.1021/acsbiomaterials.8b01131
19. Zhao Q, Yi L, Jiang L, et al. (2019) Surface functionalization of titanium with zinc/strontium-doped titanium dioxide microporous coating via microarc oxidation. *Nanomedicine* 16: 149–161. https://doi.org/10.1016/j.nano.2018.12.006
20. Pan YK, Chen CZ, Wang DG, et al. (2013) Preparation and bioactivity of micro-arc oxidized calcium phosphate coatings. *Mater Chem Phys* 141: 842–849. https://doi.org/10.1016/j.matchemphys.2013.06.013
21. Sedelnikova MB, Sharkeev YP, Komarova EG, et al. (2016). Structure and properties of the wollastonite–calcium phosphate coatings deposited on titanium and titanium–niobium alloy using microarc oxidation method. *Surf Coat Technol* 307: 1274–1283. https://doi.org/10.1016/j.surfcoat.2016.08.062
22. Wang Y, Yu D, Ma K, et al. (2023) Self-healing performance and corrosion resistance of a bilayer calcium carbonate coating on microarc-oxidized magnesium alloy. *Corros Sci* 212: 110927. https://doi.org/10.1016/j.corsci.2022.110927
23. Muhaffel F, Cimenoglu H (2019) Development of corrosion and wear resistant micro-arc oxidation coating on a magnesium alloy. *Surf Coat Technol* 357: 822–832. https://doi.org/10.1016/j.surfcoat.2018.10.089
24. Rakhadilov BK, Baizhan DR, Sagdoldina ZB, et al. (2022) Research of regimes of applying coats by the method of plasma electrolytic oxidation on Ti-6Al-4V. *Bull Karaganda Univ* 105: 99–106. https://doi.org/10.31489/2022ph1/99-106
25. Baizhan DR, Rakhadilov BK, Aldabergenova TM, et al. (2023) Obtaining of calcium-phosphate coatings on the titanium surface by micro-arc oxidation. *Eurasian Phys Tech J* 20: 34–41. https://doi.org/10.31489/2023No1/34-41
26. Saikiran A, Hariprasad S, Arun S, et al. (2019) Effect of electrolyte composition on morphology and corrosion resistance of plasma electrolytic oxidation coatings on aluminized steel. *Surf Coat Technol* 372: 239–251. https://doi.org/10.1016/j.surfcoat.2019.05.047
27. Toulabifard A, Rahmati M, Raeissi K, et al. (2020) The effect of electrolytic solution composition on the structure, corrosion, and wear resistance of PEO coatings on AZ31 magnesium alloy. *Coatings* 10: 937. https://doi.org/10.3390/coatings10100937
28. Wu T, Blawert C, Serdechnova M, et al. (2022) Role of phosphate, silicate and aluminate in the electrolytes on PEO coating formation and properties of coated Ti6Al4V alloy. *Appl Surf Sci* 595: 153523. https://doi.org/10.1016/j.apsusc.2022.153523
29. Wu T, Blawert C, Serdechnova M (2022) Formation of plasma electrolytic oxidation coatings on pure niobium in different electrolytes. *Appl Surf Sci* 573: 151629. https://doi.org/10.1016/j.apsusc.2021.151629
30. Zehra T, Kaseem M, Hossain S, et al. (2021) Fabrication of a protective hybrid coating composed of TiO_2, MoO_2, and SiO_2 by plasma electrolytic oxidation of titanium. *Metals* 11: 1182. https://doi.org/10.3390/met11081182

31. Kaseem M, Choe HC (2021) The effect of in-situ reactive incorporation of MoOx on the corrosion behavior of Ti-6Al-4V alloy coated via micro-arc oxidation coating. *Corros Sci* 192: 109764. https://doi.org/10.1016/j.corsci.2021.109764
32. Molaei M, Fattah-Alhosseini A, Nouri M, et al. (2023) Role of TiO_2 nanoparticles in wet friction and wear properties of PEO coatings developed on pure titanium. *Metals* 13: 821. https://doi.org/10.3390/met13040821
33. Kim SP, Kaseem M, Choe HC (2020) Plasma electrolytic oxidation of Ti-25Nb-xTa alloys in solution containing Ca and P ions. *Surf Coat Technol* 395: 125916. https://doi.org/10.1016/j.surfcoat.2020.125916
34. Kasatkin VE, Kasatkina IV, Bogdashkina NL, et al. (2023) Influence of different modes of microarc oxidation of titanium on the electrochemical properties and surface morphology of the obtained coatings. *Surf Eng* 39: 295–306. https://doi.org/10.1080/02670844.2023.2223451
35. Bayatanova LB, Zhassulankyzy AZ, Magazov NM, et al. (2023) Effect of plasma-electrolytic oxidation on mechanical properties of titanium coatings. *Bull Karaganda Univ* 111: 65–74. https://doi.org/10.31489/2023ph3/65-74
36. Kuroda PA, de Mattos FN, Grandini CR, et al. (2023) Effect of heat treatment on the phases, pore size, roughness, wettability, hardness, adhesion, and wear of Ti-25Ta MAO coatings for use as biomaterials. *J Mater Sci* 58: 15485–15498. https://doi.org/10.1007/s10853-023-08979-2
37. Ding H (2010) Corrosion wear behaviors of micro-arc oxidation coating of Al_2O_3 on 2024Al in different aqueous environments at fretting contact. *Tribol Int* 43: 868–875. https://doi.org/10.1016/j.triboint.2009.12.022
38. Zhang D (2018) Investigation of tribological properties of micro-arc oxidation ceramic coating on Mg alloy under dry sliding condition. *Ceram Int* 44: 16164–16172. https://doi.org/10.1016/j.ceramint.2018.05.137
39. Song SJ, Fan XQ, Yan H, et al. (2023) Facile fabrication of continuous graphene nanolayer in epoxy coating towards efficient corrosion/wear protection. *Compos Commun* 37: 101437. https://doi.org/10.1016/j.coco.2022.101437
40. Zhang G, Huang S, Li X, et al. (2023) Oxide ceramic coatings with amorphous/nano-crystalline dual-structures prepared by micro-arc oxidation on Ti–Nb–Zr medium entropy alloy surfaces for biomedical applications. *Ceram Int* 49: 18114–18124. https://doi.org/10.1016/j.ceramint.2023.02.180
41. Sharkeev Y, Komarova E, Sedelnikova M, et al. (2019) Bioactive micro-arc calcium phosphate coatings on nanostructured and ultrafine-grained bioinert metals and alloys, In: Antoniac L, *Bioceramics and Biocomposites: From Research to Clinical Practice*, New York: John Wiley & Sons, 191–231. https://doi.org/10.1002/9781119372097.ch8
42. Xie NS, Wang J (2014) Study on properties of Al_2TiO_5 coating on Ti-6Al-4V titanium alloy. *Key Eng Mater* 575–576: 348–351. https://doi.org/10.4028/www.scientific.net/KEM.575-576.348
43. Ma S, Wang T, Qian L, et al. (2018) Microstructure and corrosion properties of ZK60 alloys modified by micro-arc oxidation coatings using phosphate-borate electrolyte in KOH solution. *Int J Electrochem Sci* 13: 6451–6461. https://doi.org/10.20964/2018.07.13
44. Joni MS, Fattah-alhosseini A (2016) Effect of KOH concentration on the electrochemical behavior of coatings formed by pulsed DC micro-arc oxidation (MAO) on AZ31B Mg alloy. *J Alloys Compd* 661: 237–244. https://doi.org/10.1016/j.jallcom.2015.11.169

45. Muhaffel F, Jarzębska A, Trelka A, et al. (2024) Unveiling the mechanisms of coating formation during micro-arc oxidation of titanium in Na_2HPO_4 electrolyte. *Surf Coat Technol* 476: 130224. https://doi.org/10.1016/j.surfcoat.2023.130224
46. Terleeva OP, Sharkeev YP, Slonova AE, et al. (2010) Effect of microplasma modes and electrolyte composition on micro-arc oxidation coatings on titanium for medical applications. *Surf Coat Technol* 205: 1723–1729. https://doi.org/10.1016/j.surfcoat.2010.10.019
47. Rakhadilov BK, Kovalevsky P, Baizhan DR, et al. (2022) Investigation of the modes of oxide coating on titanium Ti-6AL-4V by plasma-electrolytic oxidation. *Bull D Serikbayev East Kazakhstan State Tech Univ* 1: 100–111. https://doi.org/10.51885/1561-4212_2022_1_100
48. Collins TJ (2007) ImageJ for microscopy. *Biotechniques* 43: S25–S30. https://doi.org/10.2144/000112517
49. Kulkov AS, Smolin IY, Mikushina VA (2019) Structural features of porous ceramics obtained at different sintering temperatures. International Conference and the VIII All-Russian Scientific and Practical Conference with international participation, dedicated to the 50th anniversary of the founding of the Institute of Petroleum Chemistry, National Research Tomsk State University，Tomsk. https://doi.org/10.17223/9785946218412/93
50. Dudareva NY, Kolomeichenko AV, Deev VB, et al. (2022) Porosity of oxide ceramic coatings formed by micro-arc oxidation on high-silicon aluminum alloys. *J Surf Investig* 16: 1308–1314. https://doi.org/10.1134/S1027451022060362
51. Sharkeev YP, Komarova EG, Chebodaeva VV, et al. (2021) Amorphous–crystalline calcium phosphate coating promotes in vitro growth of tumor-derived jurkat T cells activated by anti-CD2/CD3/CD28 antibodies. *Materials* 14: 3693. https://doi.org/10.3390/ma14133693
52. Komarova EG, Sharkeev YP, Sedelnikova MB, et al. (2020) Zn-or Cu-containing CaP-based coatings formed by micro-arc oxidation on titanium and Ti-40Nb alloy: Part I—Microstructure, composition and properties. *Materials* 13: 4116. https://doi.org/10.3390/ma13194366
53. Sharkeev Y, Komarova E, Sedelnikova M, et al. (2017) Structure and properties of micro-arc calcium phosphate coatings on pure titanium and Ti–40Nb alloy. *T Nonferr Metal Soc* 27: 125–133. https://doi.org/10.1016/s1003-6326(17)60014-1
54. Glazov IE, Krut'ko VK, Musskaya ON, et al. (2022) Calcium phosphate apatites: wet formation, thermal transformations, terminology, and identification. *Russ J Inorg Chem* 67: 173–182. https://doi.org/10.1134/S0036023622020048
55. Matykina E, Arrabal R, Mohedano M, et al. (2013) Stability of plasma electrolytic oxidation coating on titanium in artificial saliva. *Mater Sci: Mater Med* 24: 37–51. https://doi.org/10.1007/s10856-012-4787-z
56. Sodium phosphate (Na_3PO_4)—Molecular mass, structure, properties and uses. Available from: https://byjus.com/chemistry/sodium-phosphate/.
57. Blau P (2001) The significance and use of the friction coefficient. *Tribol Int* 34: 585–591. https://doi.org/10.1016/S0301-679X(01)00050-0
58. Cheng YH, Browne T, Heckerman B, et al. (2011) Influence of the C content on the mechanical and tribological properties of the TiCN coatings deposited by LAFAD technique. *Surf Coat Technol* 205: 4024–4029. https://doi.org/10.1016/j.surfcoat.2011.02.032

59. Martínez AL, Flamini DO, Saidman SB (2022) Corrosion resistance improvement of Ti-6Al-4V alloy by anodization in the presence of inhibitor ions. *Trans Nonferrous Met Soc China* 32: 1896–1909. https://doi.org/10.1016/S1003-6326(22)65917-X

AIMS Press